JMJD3 Is Required for Acute Pancreatitis and Pancreatitis-Associated Lung Injury

Li Chen,*[,1] Xiangxian Zhang,*[,1] Yu Liu,*[,1] Li Liu,* Xiao Liang,* Shengqun Yang,* Qing Xia,[†] Tao Jin,[†] Yun Ma,[†] Yonghua Chen,[‡] Xia Yuan,* Yan Tie,* Yangzhuo Gu,* Chunju Fang,* Siyuan Chen,* Fei Mo,* Ting Yu,* Yuzhu Hu,* Zhiyong Qian,* Yong Peng,* Jia Geng,* Zongguang Zhou,[§] Min Wu,[¶] Jiansheng Ding,[‖] Daoke Yang,[‖] and Xiawei Wei*

Acute pancreatitis (AP) can be complicated by inflammatory disorders of remote organs, such as lung injury, in which Jumonji domain-containing protein 3 (JMJD3) plays a vital role in proinflammatory responses. Currently, we found that JMJD3 expression was upregulated in the pancreas and lung in an AP male mouse model, which was also confirmed in AP patients. Further experiments revealed that the upregulation of JMJD3 and proinflammatory effects were possibly exerted by mitochondrial DNA (mtDNA) or oxidized-mtDNA from tissue injury caused by AP. The release of mtDNA and oxidized-mtDNA contributed to the infiltration of inflammatory monocytes in lung injury through the stimulator of IFN genes (STING)/TLR9-NF-κB-JMJD3-TNF-α pathway. The inhibition of JMJD3 or utilization of *Jmjd3-cKO* mice significantly alleviated pulmonary inflammation induced by AP. Blocking mtDNA oxidation or knocking down the TLR9/STING pathway effectively alleviated inflammation. Therefore, inhibition of JMJD3 or STING/TLR9 pathway blockage might be a potential therapeutic strategy to treat AP and the associated lung injury. ***The Journal of Immunology*****, 2023, 210: 180–190.**

Acute pancreatitis (AP) is an acute inflammatory disorder of the pancreas that can be complicated by the involvement of other remote organs. The current strategy of treatment in AP is limited to supportive care, adequate analgesia, and treatment of complications when they develop (1–4). The morbidity and mortality of severe AP are determined largely by the extent of the related inflammatory response (2–4). Multiple organ dysfunction syndromes will occur if the patients' systemic inflammatory response gets worse (2–4). Severe AP with severe complications such as multiple organ failure often gives rise to high mortality (30–40%) despite intensive treatment (2, 4). Therefore, there is still an urgent need for novel approaches to better control inflammation in severe clinical conditions (2, 5). However, the molecular mechanism regulating the inflammatory response in the pancreas and other remote organs remains poorly understood.

Lysine-specific demethylase Jumonji domain-containing protein 3 (JMJD3), also known as lysine-specific demethylase 6B, is an important histone demethylase that enhances gene expression by demethylating the repressive epigenetic marker, H3K27me3 (trimethyl-lysine 27 on histone H3), in genes (6). A large number of studies have shown that JMJD3 promotes inflammatory diseases by enhancing proinflammatory gene expression (7). JMJD3 binds to Polycomb group target genes and demethylates H3K27me3 into dimethyl-lysine 27 on histone H3 (H3K27me2)/H3K27me to enable or enhance transcriptional activation of target genes (H3K27me2/3) (8). JMJD3 has been proven to promote TNF-α gene transcription by demethylating H3K27me3 from the TNF-α transcription start site to enhance the binding of RNA polymerase II (9).

AP is characterized by inflammatory disease with a significant increase in proinflammatory cytokines such as TNF-α, IL-1, and IL-6 (10). TNF-α, the cell death–inducing cytokine, is mainly produced by monocytes and macrophages. It has been proven to induce inflammatory gene upregulation, endothelial upregulation, cell death, and the recruitment and activation of immune cells in the pathogenesis of AP (11).

*Laboratory of Aging Research and Nanotoxicology, State Key Laboratory of Biotherapy, West China Hospital, National Clinical Research Center for Geriatrics, West China Hospital, Sichuan University, Chengdu, Sichuan, People's Republic of China; [†]Department of Integrated Traditional Chinese and Western Medicine, West China Hospital, Sichuan University, Chengdu, Sichuan, People's Republic of China; [‡]Department of Pancreatic Surgery/Pancreatic Disease Center, West China Hospital, Sichuan University, Chengdu, Sichuan, People's Republic of China; [§]Department of Gastrointestinal Surgery, West China Hospital, Sichuan University, Chengdu, Sichuan, People's Republic of China; [¶]Department of Biochemistry and Molecular Biology, School of Medicine and Health Sciences, University of North Dakota, Grand Forks, ND; and [‖]Department of Radiotherapy, The First Affiliated Hospital of Zhengzhou University, Zhengzhou, China

[1]L.C., X.Z., and Y.L. contributed equally to this work.

ORCIDs: 0000-0003-0330-7027 (X.L.); 0000-0001-8485-0755 (Y.C.); 0000-0003-4096-8975 (T.Y.); 0000-0002-1181-3467 (Y.P.); 0000-0002-6513-6422 (X.W.).

Received for publication July 8, 2022. Accepted for publication November 1, 2022.

This work was supported by Ministry of Science and Technology of the People's Republic of China, National Key Research and Development Program of China Grant 2016YFA0201402.

X.W. conceived the research and designed the experiments; X.W. wrote the manuscript; L.C. and X.Z. illustrated the figures; L.C., X.Z., and Y.L. performed the experiments and analyzed the original data; L.L., X.L., S.Y., Q.X., T.J., Y.M., Y.C., X.Y., Y.T., Y.G., C.F., S.C., F.M., T.Y., and Y.H. revised the manuscript; Z.Q., Y.P., J.G., Z.Z., M.W., J.D., and D.Y. analyzed and interpreted the data and assisted with the adjustments of directions and interpretation of the mechanistic aspects of the results. All authors approved the final manuscript.

Address correspondence and reprint requests to Prof. Xiawei Wei, Laboratory of Aging Research and Nanotoxicology, State Key Laboratory of Biotherapy, National Clinical Research Center for Geriatrics, West China Hospital, Sichuan University, No. 17, Block 3, Southern Renmin Road, Chengdu, Sichuan 610041, People's Republic of China. E-mail address: xiaweiwei@scu.edu.cn

The online version of this article contains supplemental material.

Abbreviations used in this article: AP, acute pancreatitis; Cae, caerulein; Cat #, catalog number; CP, chronic pancreatitis; DAMP, damage-associated molecular pattern; H3K27me3, trimethyl-lysine 27 on histone H3; JMJD3, Jumonji domain-containing protein 3; L-Arg, L-arginine; mtDNA, mitochondrial DNA; NAC, *N*-acetylcysteine; NS, normal saline; ODN, oligodeoxynucleotide; 8-OHdG, 8-hydroxy-2-deoxyguanosine; qPCR, quantitative PCR; ROS, reactive oxygen species; STING, stimulator of IFN genes.

The NF-κB and MAPK signaling pathways are critical for TNF-α production in response to TLR and stimulator of IFN genes (STING) stimulation (12, 13). NF-κB, a nuclear transcription factor responsible for upregulating the transcription of a wide variety of inflammatory genes including TNF-α, has been shown to promote the development of AP (14). NF-κB also rapidly stimulated JMJD3 expression by binding to a cluster of three κB sites in the JMJD3 gene promoter in LPS-stimulated macrophages (15), indicating the relationship between epigenetic regulation and inflammation. In HUVECs, LPS induced the enrichment of NF-κB/p65 and JMJD3 to the promoter regions of TNF-α (15). Interestingly, JMJD3 was identified by chromatin immunoprecipitation sequencing to stimulate the genes involved in NF-κB activation (16), and TNF-α is also an activator of NF-κB (17). Thus, NF-κB, JMJD3, and TNF-α form a positive feedback loop to promote each other's transcription. It is conceivable that the inhibition of JMJD3 expression inhibits the positive feedback loop and plays an effective therapeutic role in inflammatory diseases.

Acinar cell death is critical to AP. Dying acinar cells release damage-associated molecular patterns (DAMPs), which might contribute to pancreatic injury, proinflammatory cytokine release, and remote organ injury through specific DAMP receptors, such as TLR and STING (18). Mitochondrial DNA (mtDNA), an important source of DAMPs, was reported to induce an inflammatory response after injury through the STING and TLR9 pathways (19, 20). In addition, the oxidation of mtDNA could be induced by reactive oxygen species (ROS) generation in cell stress or infiltrating inflammatory cells, which can be recognized as a potent DAMP with a more significant potential to trigger innate immune responses through the STING and TLR9 pathways (21–23).

Considering the vital role of JMJD3 and mtDNA or oxidized-mtDNA in the regulation of the inflammatory response, we hypothesize that mtDNA and oxidized-mtDNA released from acinar cell death in AP may upregulate the expression of JMJD3, which in turn triggers the inflammatory response in pancreatic tissues and pancreatitis-associated lung injury. To test this concept, we used AP male mouse models induced by L-arginine (L-Arg) and caerulein (Cae), as well as human tissues from chronic pancreatitis (CP) patients, to investigate the possible role of JMJD3, mtDNA, and oxidized-mtDNA in the regulation of the inflammatory process of AP and the underlying mechanism.

Materials and Methods

Patients

AP patients admitted to West China Hospital of Sichuan University from January 2019 to May 2019 were enrolled. Inclusion criteria were (1) 18–45 y old and (2) met the 2012 Atlanta diagnostic revision for AP (24). Exclusion criteria were (1) gravidas and children; (2) patients with myocardial infarction, malignant diseases, end-stage liver disease, renal disease or organ failure, among others; and (3) the hospitalization admission was <24 h. In addition, physical examination individuals without any disease at the health management center were enrolled in the control group. Afterward, peripheral blood samples were acquired. All patients signed the informed consent form, which was approved by the West China Hospital Ethics Committee.

Mice

Male C57BL/6 mice, 20–25 g, were obtained from Beijing Huafukang Biotechnology Co. The experimental animal program was approved by the Committee for Animal Protection and Utilization of Sichuan University. All experiments followed the principles of laboratory animal protection. In selected experiments, C57BL/6 mice with global deletion of TLR9 (obtained from Bioindustry Division Oriental Yeast Co.) and STING (obtained from The Jackson Laboratory) expression were also used. *Jmjd3-cKO* mice were generated by targeting exons 15–21 (encoding the JmjCcatalytic domain) using a Cre-LoxP system. All animal experiments were approved by the Committee on Animal Protection and Utilization and the Ethics Committee.

Induction of pancreatitis

Pancreatitis was induced by i.p. injection of the cholecystokinin analog Cae at seven doses of 50 μg/kg each, 1 h apart (25). L-Arg hydrochloride sterile solution (8%) was prepared in normal saline (NS; pH 7.0), and the nonfasted mice were i.p. injected with L-Arg hydrochloride sterile solution in two doses of 4 g/kg each, 1 h apart. The control group received only aseptic saline injections (26). For administration of GSK-J4 (Sigma), mice were divided into four groups: NS group, AP model group treated with Cae, AP model group treated with 20 mg/kg (50 mg/kg in Cae-induced AP group) GSK-J4, and AP model group treated with 50 mg/kg (100 mg/kg in Cae-induced AP group) GSK-J4. For AP-induced mice with L-Arg, GSK-J4 was injected i.p. in two doses, 20 and 50 mg/kg, at 24, 48, and 72 h after the first injection of L-Arg. For AP-induced mice with Cae, GSK-J4 was injected i.p. in two doses, 50 and 100 mg/kg at 3, 8, 24, 48, and 72 h after the first administration of Cae. The *N*-acetylcysteine (NAC) injection schedule was the same as GSK-J4, and both AP models were injected with 300 mg/kg NAC i.p. each time.

Detection of inflammatory neutrophils, monocytes, and intracellular monocyte TNF-α by flow cytometry

To detect monocytes and neutrophils infiltrating the pancreas, lung, and peripheral blood, we processed the samples as described previously (19, 26–28). Cells were dispersed in PBS at 1×10^6 cells/100 μl and stained with allophycocyanin-rat anti-mouse CD45 (1:100, catalog number [Cat #] 147708; BioLegend), PerCP-Cy5.5 rat anti-mouse CD11b (1:100, Cat #101228; BioLegend), PE-rat anti-mouse Ly6G (1:100, Cat #127608; BioLegend), and FITC-rat anti-mouse Ly6C (1:100, Cat #128005; BioLegend) Abs and then measured by flow cytometry for the detection of monocytes in human peripheral blood. We used allophycocyanin-mouse anti-human HLA-DR (1:100, Cat #307610; BioLegend), PerCP-Cy5.5 mouse anti-human CD16 (1:100, Cat #302028; BioLegend), and PE-mouse anti-human CD14 (1:100, Cat #367104; BioLegend) Abs and then measured the cells by flow cytometry (29). Intracellular monocyte TNF-α was detected as previously described (30).

Isolation of monocytes and neutrophils from mouse bone marrow and peripheral blood

Monocytes and neutrophils from mouse bone marrow and peripheral blood were prepared as previously described (26). More than 85% of the separated cells were monocytes or neutrophils, as determined by flow cytometry.

Quantitative real-time PCR for JMJD3 and mtDNA

Total RNA was extracted from the pancreas, lung, and isolated monocytes using an RNA Simple Total RNA Kit (TIANGEN, Beijing, China). A PrimeScript RT kit with a genomic DNA eraser (Perfect Real Time; Takara, Dalian, China) was used to synthesize the first complementary strand of DNA from the total RNA template. The resulting cDNA was added and mixed into iQ SYBR Green Supermix (perfect real-time; Bio-Rad) in a CFX96 Real-Time PCR Detection System (Bio-Rad, Hercules, CA) according to the manufacturer's protocol. The expression levels of the target genes were standardized to that of GAPDH. The mtDNA in the serum of mice and humans was concentrated and purified by a QIAamp DNA Blood Mini Kit (Qiagen). Then, mtDNA was quantified with a TaqMan probe. The PCR primers, probes, and the standard curve of mice used to amplify mouse mtDNA were designed as described previously (19). Primers were synthesized by Invitrogen. The standard samples, PCR primers, and probes of human mtDNA were designed and synthesized by Molecular Biotechnology Co. (Tianjin, China). All primer sequences quantitative PCR (qPCR) were as follows: GAPDH (mouse), forward 5′-ACCCAGAAGACTGTGGATGG-3′, reverse 5′-ACATTGGGG GTAGGAACAC-3′; JMJD3 (mouse), forward 5′-CCCCCATTTCAGCTGACTAA-3′, reverse 5′-CTGGACCAAGGGGTGTGTT-3′; homo-GAPDH, forward 5′-CTGATGCCCCCATGTTCGTC-3′, reverse 5′-CACCCTGTTGCTGATGCCAAATTC-3′; homo-JMJD3, forward 5′-TGTTCCCTGTAGCACATCAAG-3′, reverse 5′-TAGAGTGAGTGCGTTTCG-3′; mtDNA (mouse), forward 5′-ACCTACCCTATCACTCACACTAGCA-3′, reverse 5′-GAGGCTCATCCTGATCATAGAA TG-3′; FAM-labeled TAMRA-quenched probes (mouse), 5′-ATGAGTTCCCCTACCAATACCACACCC-3′; homo-mtDNA, forward 5′-CCCCACATTAGGCTTAAAAACAGAT-3′, reverse 5′-TATACCCCC GGTCGTGTAGCGGT-3′; FAM-labeled TAMRA-quenched probes (human), 5′-CAATTCCCGGACGTCTAAACCAC-3′.

Esterase staining and immunofluorescence

Esterase staining was performed by staining with a Naphthol AS-D Chloroacetate kit (Sigma) following the instructions. Immunofluorescence of JMJD3 expression in monocytes in the pancreas and lung was detected in frozen tissue sections that were prepared as previously described (31). Frozen tissue sections were coimmunostained with rabbit anti-JMJD3 (1:400, Cat #GTX31466; GeneTex) and rat anti-mouse Ly6C (1:400, ab24973; Abcam)

Abs, followed by a Cy3-conjugated goat anti-rabbit secondary Ab (1:200, ab6939; Abcam) and Alexa 488 goat anti-rat secondary Ab (1:200, ab150081; Abcam). The 8-hydroxy-2-deoxyguanosine (8-OHdG) index was stained with goat 8-OHdG (1:200, ab93295; Abcam) and rabbit anti-mouse/human TOMM 20 (1:250, ab186734; Abcam) Abs, followed by Alexa Fluor 647 donkey anti-rabbit secondary Ab (1:200, ab150075; Abcam) and Alexa 488 donkey anti-goat secondary Ab (1:400, ab150129; Abcam). The nucleus was stained with Hoechst 33342 (20 μg/ml; Sigma) for 30 min. Images were captured by using the Zeiss LSM880 confocal microscope. ROS production was measured in situ on pancreas slices as previously described (32). We used a fluorescent ROS probe, H_2DCFDA (Invitrogen), which is a substrate without fluorescence itself that converts to a green fluorescent product when it is hydrolyzed by intracellular esterase.

Pancreatic severity assessment

Pancreatic and pulmonary tissues were soaked in 4% paraformaldehyde, embedded in paraffin, and then sectioned. The tissue sections were stained with H&E to accurately assess the extent of tissue injury. The histopathological scoring analysis of the pancreas and lung was performed blindly by three independent pathologists following a corresponding scoring system based on previous studies (33, 34).

Isolation of pancreatic cells

Pancreatic cells were obtained by a modified digesting and suspending technique as previously described (35). For the treatment of pancreatic cells with L-Arg in vitro, the isolated pancreatic cells were incubated with 10 mg/ml L-Arg in DMEM supplemented with 10% FBS, 1000 U/ml penicillin G, 100 μg/ml streptomycin, and 0.1 mg/ml soybean trypsin inhibitor (Sigma) for 12 h, and the necrosis rate of the separated cells was >75% (36). For the treatment of pancreatic cells with Cae in vitro, the isolated pancreatic cells were incubated with 100 μg/ml Cae for 24 h, and the cell death rate was nearly 30% (37).

Preparation of mitochondria, mtDNA, and oxidized-mtDNA

mtDNA was isolated from the pancreas of C57BL/6 mice by an mtDNA isolation kit (ab65321; Abcam) under sterile conditions. The concentration of mtDNA was detected by a spectrophotometer; there was no protein contamination. The mtDNA was stored in sterile water and kept at −80°C for long-term storage. Mitochondria were isolated by a mitochondria isolation kit (MITOISO2; Sigma). The endotoxin level of mtDNA was detected at <0.25 endotoxin unit/ml. Oxidized-mtDNA was prepared by irradiating mtDNA on ice with a 254-nm germicidal UV lamp (a series of five 8-W tubes) for 0.5 h (38).

Western blot assay

mtDNA (0.5 μg/ml) and oxidized-mtDNA (0.5 μg/ml) were used to stimulate freshly isolated monocytes at a concentration of 5×10^6 cells/ml and incubated at 37°C for 0.5 h, and then monocytes were lysed to prepare protein samples. Samples containing equal amounts of protein were electrophoretically transferred onto a polyvinylidene difluoride membrane and then blocked in TBST buffer containing 5% skim milk. Abs to phospho-p38 MAPK (Thr 180/Tyr 182; #4511; Cell Signaling Technology), p38 MAPK (#8690; Cell Signaling Technology), NF-κB p65 (#8242; Cell Signaling Technology), phospho-NF-κB p65 (#3033; Cell Signaling Technology), β-actin (ab179467; Abcam), and JMJD3 (1:1000 for all; GeneTex) were used. The polyvinylidene difluoride membrane was incubated with specific primary Abs at 4°C overnight, washed with PBST, and then incubated with HRP-conjugated secondary Abs. The target proteins on the blot were visualized by a SuperSignal West Dura Substrate (Thermo Fisher Scientific, Waltham, MA).

Measurement of 8-OHdG

The 8-OHdG levels in mouse and human serum were measured using a commercial 8-OHdG ELISA kit (Abcam) following the instructions. The concentration (ng/ml) was measured at 450 nm.

Statistical analyses

Groups were compared with Prism software (GraphPad) using a 11122eq two-tailed unpaired Student *t* test or one-way ANOVA. Data are presented as the means ± SEM.

Results

JMJD3 expression was upregulated in monocytes of mice/patients with AP

To study the role of JMJD3 in AP, we established a mouse model of AP by injecting L-Arg or Cae in previous reports (25, 26). As shown in Fig. 1A, 96 h after the repetitive injection of L-Arg and 48 h after the injection of Cae in mice, significant morphological damage was observed in the pancreas and lung of AP mice by H&E histology staining. The pathomorphological changes in the pancreas of AP mice, including acinar cell necrosis, edema, and inflammatory cell infiltration, were significantly more severe than those in the control group (Fig. 1A, left, Supplemental Figs. 2A, 4A). The lungs of AP mice showed an extreme inflammatory response by an abundance of inflammatory cells (Fig. 1A, right, Supplemental Figs. 2A, 4A). The expression and distribution of JMJD3 in the AP model (Fig. 1B, Supplemental Fig. 4F) were further detected, and the expression level of JMJD3 in the pancreatic tissue (Fig. 1C) and the isolated peripheral blood monocytes (Fig. 1D) was increased in the AP mice as detected by Western blot and qPCR. In addition, the percentage of infiltrating inflammatory TNF-α^+ monocytes was increased in the pancreas of AP mice at 24 h after the first injection of L-Arg and Cae by intracellular staining of TNF-α (26) (Fig. 1E). Eight hours after the first injection of L-Arg or Cae, JMJD3 was upregulated in the monocytes infiltrating in the pancreas in the AP group and was predominantly distributed in the nuclei of monocytes as detected by immunofluorescent staining (Fig. 1F).

Peripheral blood samples of 18 patients admitted to West China Hospital within 24 h from the onset of symptoms and diagnosed with AP and pancreatic tissue from 4 patients with CP were collected to explore the effects of JMJD3 in human pancreatitis. The control group included 18 age-matched healthy volunteers. We detected the expression of JMJD3 in the human pancreas by immunofluorescent staining and found that JMJD3 expression was upregulated (Fig. 1G). Next, we observed a significant increase in the expression of JMJD3 in the peripheral blood of the AP group by qPCR (Fig. 1H). Furthermore, the percentage of HLA-DR$^+$CD16$^+$CD14$^+$ inflammatory monocytes in the peripheral blood of AP patients was increased (Fig. 1I). We observed the percentage of TNF-α^+HLA-DR$^+$CD16$^+$CD14$^+$ monocytes in the peripheral blood of the AP group by flow cytometry. The percentage of TNF-α^+HLA-DR$^+$CD16$^+$CD14$^+$ monocytes in the peripheral blood of the AP group was increased compared with that of the control group (Fig. 1J). These results indicated that JMJD3 might play a crucial role in the progression of AP.

Oxidized-mtDNA was increased in mice/patients with AP

Tissue damage by trauma or pathogenesis might release DAMPs from necrotic/necroptotic cells. Cell death and tissue damage were observed by H&E staining of the pancreas and lung of AP mice (Fig. 1A). Accordingly, the increased release of mtDNA was also detected in the patients with AP, as well as in the mouse model of AP (Fig. 2A, 2B). The tissue injury was also accompanied by the generation of ROS, which was confirmed in this study 48 h after the first injection of Cae (Supplemental Fig. 1A). Oxidative stress occurs in the development of AP in acinar cells, and excessive generation of ROS damages acinar cells via oxidation of mtDNA (39). Therefore, we further characterized the generation of oxidized-mtDNA using 8-OHdG as a marker. The level of oxidized-mtDNA in the pancreas of CP patients was increased as detected by immunofluorescent staining (Fig. 2C). 8-OHdG was more concentrated in the serum of patients with AP, as detected by ELISA (Fig. 2D, top). The percentage of 8-OHdG$^+$HLA-DR$^+$CD16$^+$CD14$^+$ monocytes was detected by flow cytometry in the peripheral blood of the AP group, and it was higher than that of the control group (Fig. 2D, bottom). Similar results were obtained in the mouse model of AP. In the pancreas of AP mice, strong 8-OHdG staining colocalized with TOMM20 (a mitochondrial outer membrane protein) staining (Supplemental Fig. 1B). The result was further confirmed by flow cytometry of intracellular staining for 8-OHdG in Ly6C$^+$ inflammatory monocytes in the mouse pancreas and peripheral blood at 96 h after the injection of L-Arg or at 48 h

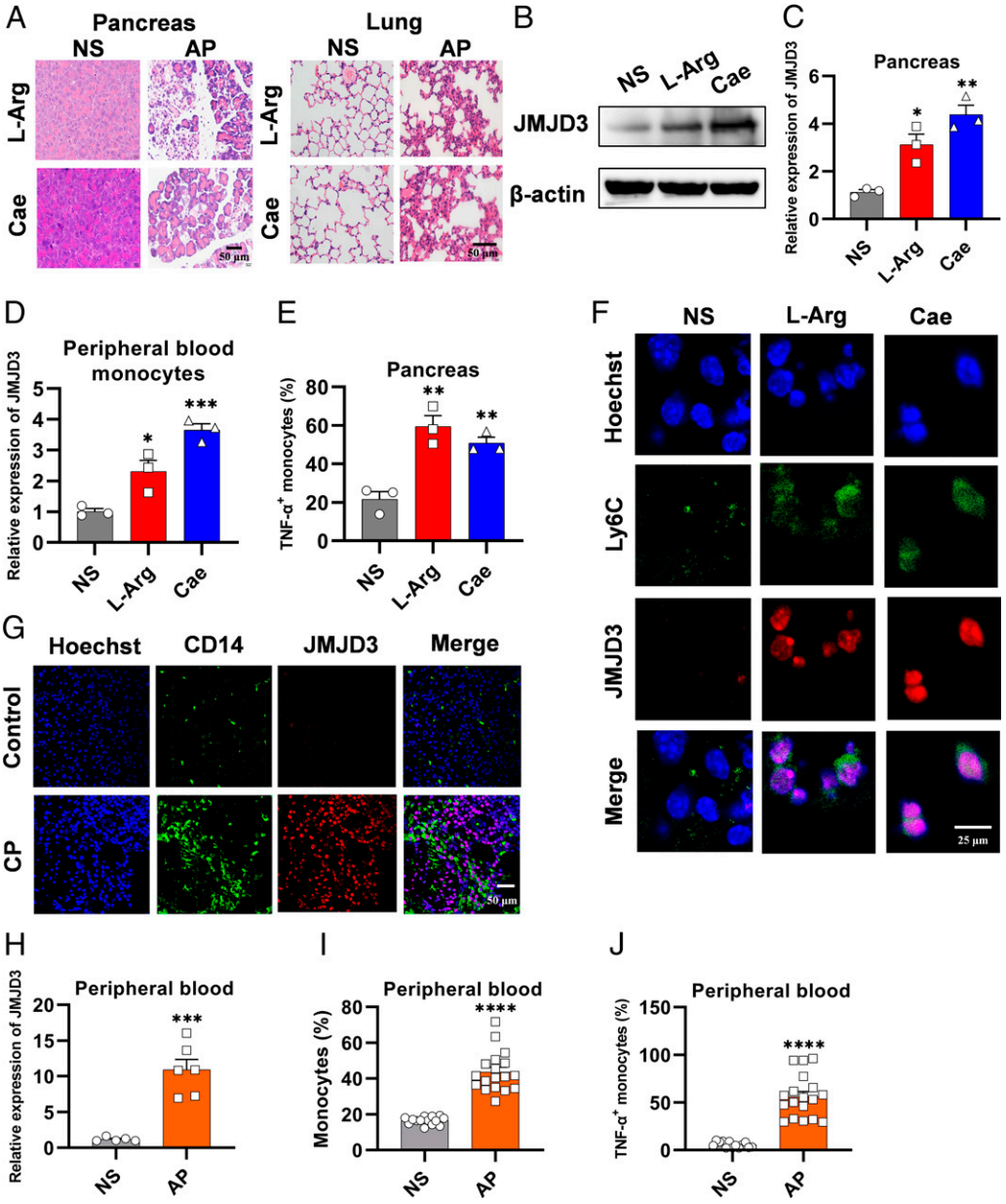

FIGURE 1. JMJD3 expression was upregulated in monocytes of mice/patients with AP. C57BL/6 mice were treated with L-Arg or Cae to induce AP, and mice in the control group received a sham injection of NS alone. (**A**) Representative H&E-stained sections of the pancreas and lung of mice at 96 h after the first injection of L-Arg and at 48 h after the first injection of Cae; original magnification ×400. (**B**) Immunoblot of JMJD3 and β-actin in the pancreas of mice at 8 h. (**C**) Relative expression of JMJD3 in the pancreas of mice at 8 h was determined by qPCR. (**D**) Relative expression of JMJD3 in the isolated peripheral blood monocytes of mice at 8 h was determined by qPCR. (**E**) Intracellular staining of TNF-α in $Ly6C^+$ inflammatory monocytes in the pancreas of mice at 24 h after the first injection of L-Arg or Cae by flow cytometry. (**F**) Immunofluorescent staining of Hoechst 33342 (blue), Ly6C (green), and JMJD3 (red) in the mouse pancreas at 8 h; original magnification ×1890. (**G**) Surgical incision tissue from four CP patients (three men and one woman; the average age was 41.25 ± 2.217 y old; the age range was 39–44 y) was provided by West China Hospital of Sichuan University. Tissue samples of four previously healthy organ donors (two men and two women; the average age was 41.75 ± 1.708 y old; the age range was 40–44 y) served as controls. Immunofluorescent staining of Hoechst 33342 (blue), CD14 (green), and JMJD3 (red) in the human pancreas; original magnification ×400. (**H**) Relative expression of JMJD3 in peripheral blood samples of healthy volunteers and AP patients. (**I**) Percentage of $HLA\text{-}DR^+CD16^+CD14^+$ inflammatory monocytes. (**J**) Intracellular staining of $TNF\text{-}\alpha^+$ inflammatory monocytes in peripheral blood samples of healthy volunteers and AP patients. Data are representative of three independent experiments, and the results are expressed as the means ± SEM. Statistical comparisons were performed using Student *t* test or one-way ANOVA (*$p < 0.05$, **$p < 0.01$, ***$p < 0.001$, ****$p < 0.0001$).

after Cae in mice (Fig. 2E). The increase of oxidized-mtDNA in isolated peripheral blood monocytes was shown by immunofluorescence in AP mice (Fig. 2F). To further confirm the key roles of cell death and mtDNA release in the progression of AP, we treated mouse peripheral blood monocytes with pancreatic acinar cells incubated with L-Arg or Cae for 6 and 8 h in vitro. In the peripheral blood monocytes treated with necrotic mouse pancreatic acinar cells, the percentage of monocytes secreting TNF-α was significantly increased compared with the control mice (Fig. 2G, top). In addition, the concentration of 8-OHdG in the serum of AP mice was higher than that in control mice (Fig. 2G, bottom). The results also showed that pancreatic acinar cells isolated from the pancreas of AP mice stimulated the secretion of TNF-α in monocytes at 6 and 8 h in vitro. These findings suggested that the release of oxidized-mtDNA was detected in the mouse

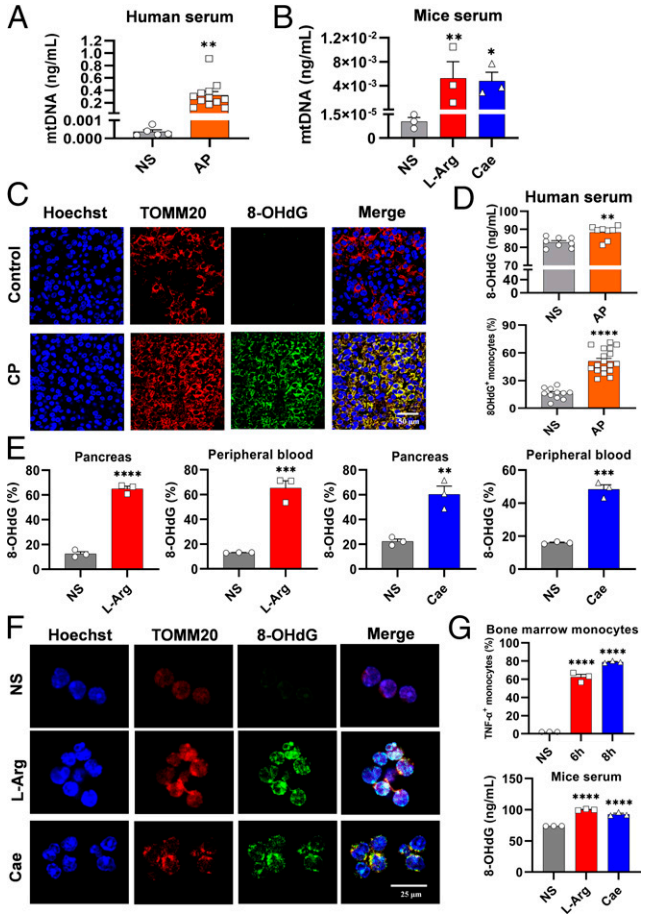

FIGURE 2. Oxidized-mtDNA was increased in mice/patients with AP. (**A**) The concentration of mtDNA in the serum of healthy volunteers and AP patients by qPCR met the criteria for AP according to the revised Atlanta classification; 12 patients (8 men and 4 women; the average age was 33.08 ± 6.775 y; the age range was 22–44 y) with confirmed AP were enrolled. The serum mtDNA levels were all measured within 24 h of hospital admission. In addition, five healthy volunteers (four men and one woman; the average age was 32.60 ± 4.159 y; the age range was 28–38 y) at the health management center were enrolled in the control group. (**B**) The concentration of mtDNA in the serum of mice was determined at 96 h after the first injection of L-Arg and at 48 h after the first injection of Cae by qPCR. (**C**) Surgical incision tissue from four CP patients (three men and one woman; the average age was 41.25 ± 2.217 y; the age range was 39–44 y) was provided by West China Hospital of Sichuan University. Tissue samples of four previously healthy organ donors (two men and two women; the average age was 41.75 ± 1.708 y; the age range was 40–44 y) served as controls. Immunofluorescent staining of Hoechst 33342 (blue), 8-OHdG (green), and TOMM20 (red) in the pancreas of healthy volunteers and CP patients; original magnification ×630. (**D**) Eight patients (six men and two women; the average age was 31.88 ± 8.823 y; the age range was 19–43 y) with confirmed AP were enrolled. The serum 8-OHdG concentration was measured by ELISA within 24 h of hospital admission. In addition, eight healthy volunteers (six men and two women; the average age was 32.25 ± 8.763 y; the age range was 18–43 y) at the health management center were enrolled in the control group (top). Eighteen patients (13 men and 5 women; the average age was 31.94 ± 7.534 y; the age range was 20–45 y) with confirmed AP were enrolled. $8\text{-OHdG}^{+}\text{HLA-DR}^{+}\text{CD16}^{+}\text{CD14}^{+}$ inflammatory monocytes in peripheral blood were measured by flow cytometry within 24 h of hospital admission. In addition, 11 healthy volunteers (8 men and 3 women; the average age was 32.82 ± 7.195 y; the age range was 21–45 y) at the health management center were enrolled in the control group (bottom). (**E**) Percentages of $8\text{-OHdG}^{+}\text{CD45}^{+}\text{CD11b}^{+}\text{Ly6C}^{+}$ inflammatory monocytes in mouse pancreas and peripheral blood at 96 h after the administration of L-Arg or 48 h after the administration of Cae, detected by flow cytometry. (**F**) Immunofluorescent staining of Hoechst 33342 (blue), TOMM 20 (red), and 8-OHdG (green) in isolated peripheral blood monocytes of mice treated with NS, L-Arg, or Cae; original magnification ×1890. (**G**) Intracellular staining of TNF-α in mouse bone marrow monocytes by flow cytometry at 6 and 8 h after coculture with L-Arg– or Cae-treated pancreatic acinar cells (top). The concentration of 8-OHdG in mouse serum by ELISA (bottom). $^{*}p < 0.05$, $^{**}p < 0.01$, $^{***}p < 0.001$, $^{****}p < 0.0001$.

model/patients with AP. Next, we tried to investigate whether the oxidized-mtDNA was associated with elevated levels of JMJD3.

mtDNA and oxidized-mtDNA stimulated the expression of JMJD3 in vitro and in vivo

In the next experiment, we studied the correlation between JMJD3 elevation and mtDNA stimulation. It is interesting to find that mtDNA or oxidized-mtDNA could induce the upregulation of JMJD3 levels both in vitro and in vivo. The incubation of mtDNA or oxidized-mtDNA with the isolated bone marrow monocytes in vitro led to a quick and significant upregulation of JMJD3 mRNA levels detected by qPCR analysis. Upregulation of JMJD3 level was detected after the stimulation for 0.5 h. It was found that oxidized-mtDNA stimulated the expression of JMJD3 more efficiently than mtDNA (Fig. 3A). On stimulation with mtDNA or oxidized-mtDNA, JMJD3 was upregulated and accumulated in the nucleus, as illustrated by immunofluorescence assay (Fig. 3B). In regard to the in vivo stimulation of mtDNA/oxidized-mtDNA to JMJD3 expression, the upregulation of JMJD3 in the pancreas of the mice in the experimental group was detected 8 h after injection (Fig. 3C). $\text{JMJD3}^{+}\text{Ly6C}^{+}$ monocytes were found in the mouse lung after the injection of mtDNA and oxidized-mtDNA (Fig. 3D). Based on this observation, the pathways involved in the upregulation of JMJD3 were characterized. The elevated protein level of JMJD3 was also confirmed after the incubation of mouse bone marrow monocytes with mtDNA and oxidized-mtDNA. In addition, the upregulation of JMJD3 protein levels was accompanied by the increased phosphorylation of MAPK p38 and NF-κB p65 in the stimulated monocytes (Fig. 3E, Supplemental Fig. 4G–I). It was reported that the activation of immune cells by mtDNA and oxidized-mtDNA was closely related to the TLR9 or STING pathway. In the next experiment, we used $Sting^{-/-}$ and $Tlr9^{-/-}$ mice to investigate whether the upregulation of JMJD3 induced by mtDNA involves these pathways. mtDNA and oxidized-mtDNA were injected i.v. into $Sting^{-/-}$ and $Tlr9^{-/-}$ mice. $Sting^{-/-}$ and $Tlr9^{-/-}$ mice showed a reduction of JMJD3 expression in the lung tissue compared with *WT* mice (Fig. 3F, 3G). The monocytes isolated from $Sting^{-/-}$ and $Tlr9^{-/-}$ mice inhibited the activation of JMJD3 induced by mtDNA and oxidized-mtDNA (Fig. 3H, Supplemental Fig. 4J–M). Therefore, our results suggested that mtDNA and oxidized-mtDNA stimulated the expression of JMJD3 in monocytes and tissues both in vitro and in vivo, which critically involves the TLR9 and STING pathways.

Mitochondrial content released by pancreatic acinar cells contributed to inflammation in mice with AP

Circulating mtDNA released from dead cells known as potent DAMPs is reported to stimulate immune cells and cause severe inflammatory response (40). Pancreatitis-associated lung injury is one of the most serious inflammatory complications of AP, and its exact mechanisms remain unclear (41). In this research, we postulated that pulmonary inflammation was partly induced by mtDNA and oxidized-mtDNA released by pancreatic acinar cells in mice with AP. To address these postulations, we isolated pancreatic acinar cells from normal mice and treated them with L-Arg or Cae in vitro for 12 or 24 h, respectively.

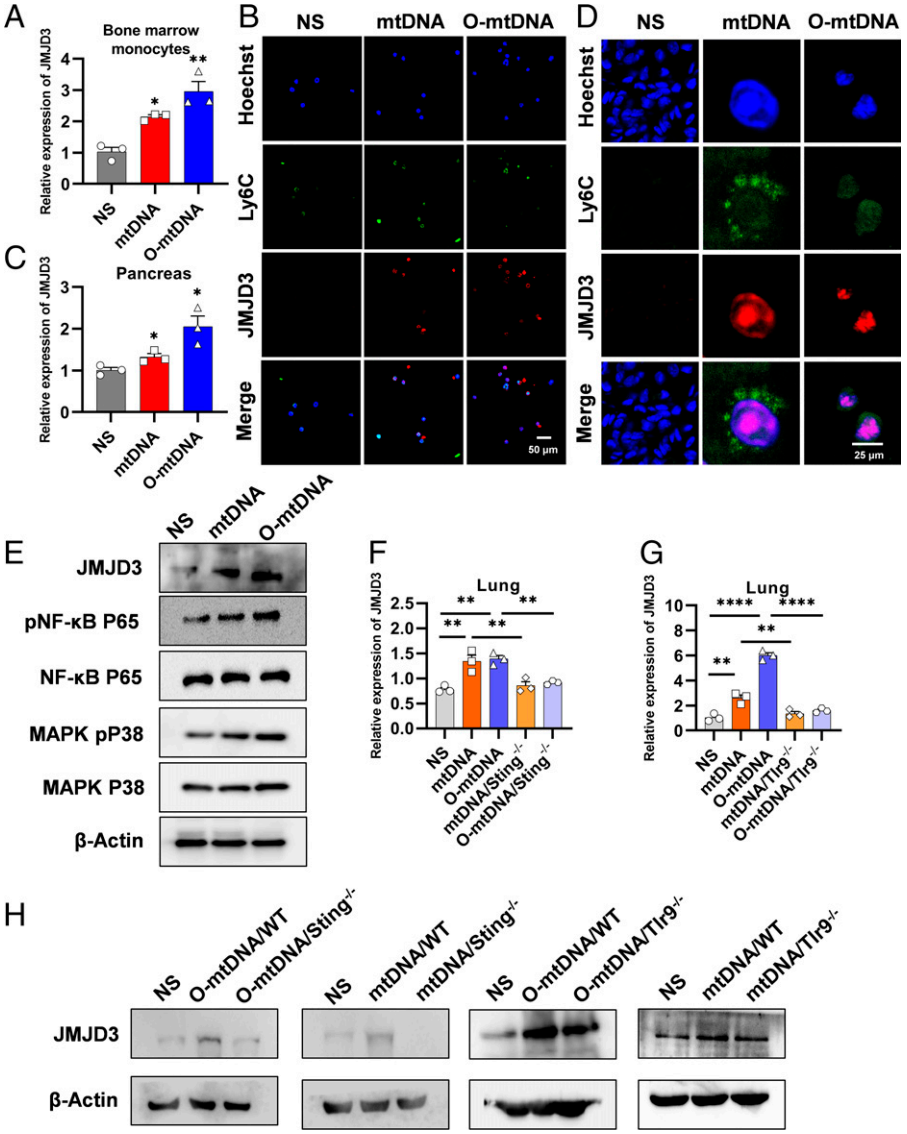

FIGURE 3. mtDNA and oxidized-mtDNA stimulated the expression of JMJD3 in vitro and in vivo. (**A**) Monocytes isolated from mouse bone marrow were stimulated with mtDNA (0.5 μg/ml) and oxidized-mtDNA (0.5 μg/ml) for 0.5 h. JMJD3 expression was detected by qPCR in vitro. (**B**) Immunofluorescent staining of Hoechst 33342 (blue), Ly6C (green), and JMJD3 (red) in mouse bone marrow monocytes; original magnification ×400. (**C**) Expression of JMJD3 was detected by qPCR in the pancreas of mice. (**D**) Mice were treated with i.v. injections of NS, mtDNA (15 μg/mouse), or oxidized-mtDNA (15 μg/mouse), and mice were sacrificed 8 h after the injection. Immunofluorescent staining of Hoechst 33342 (blue), Ly6C (green), and JMJD3 (red) in the mouse lung; original magnification ×1890. (**E**) Western blot analysis was performed to analyze the NF-κB and MAPK signaling pathways. (**F** and **G**) *WT*, *Tlr9*$^{-/-}$, and *Sting*$^{-/-}$ mice were i.v. injected with NS, mtDNA (15 μg/mouse), or oxidized-mtDNA (15 μg/mouse), and the mice were sacrificed at 8 h after the injection. The expression of JMJD3 in the mouse lung was detected by qPCR. (**H**) Monocytes isolated from the bone marrow of *WT*, *Tlr9*$^{-/-}$, and *Sting*$^{-/-}$ mice were cultured with mtDNA (0.5 μg/ml) or oxidized-mtDNA (0.5 μg/ml) for 0.5 h. Western blot of JMJD3 and β-actin was performed. $*p < 0.05$, $**p < 0.01$, $****p < 0.0001$.

Necrotic cells were also prepared through a freeze-thaw process. C57BL/6 mice were injected with NS, the pretreated pancreatic acinar cells, isolated mitochondria, mtDNA, and oxidized-mtDNA. Severe pulmonary inflammation was detected in mice 48 h after the injection of necrotic cells and all the mitochondria-derived DAMPs (Fig. 4A, Supplemental Fig. 2B). Pulmonary inflammation was further characterized by the infiltration of immune cells with esterase staining (Fig. 4B). The injection of mtDNA or oxidized-mtDNA significantly increased the percentages of TNF-α^+CD45$^+$CD11b$^+$Ly6C$^+$ inflammatory monocytes in the lung (Fig. 4C), as well as in the peripheral blood (Fig. 4D), compared with the control group. Because the oxidized-mtDNA stimulated the immune response more efficiently than the unoxidized mtDNA, we further investigated the role of mtDNA oxidation in the induction of inflammation in AP and lung injury. NAC, an ROS inhibitor, was administered to mice with AP via i.p. injection, and its influence on lung and pancreas pathology was evaluated. The percentage of CD45$^+$CD11b$^+$Ly6C$^+$ inflammatory monocytes with 8-OHdG in the L-Arg/Cae–induced mouse AP model was decreased after the injection of NAC, suggesting the efficient inhibition of cell oxidation by ROS (Fig. 4E). Treatment with NAC led to a decreased level of JMJD3 in the mouse pancreas. Because 300 mg/kg NAC was administered i.p. 3 h after the first administration of L-Arg or Cae, the level of JMJD3 significantly decreased in the tissue of the AP model group as detected at 8 h (Fig. 4F), which is consistent with our hypothesis that oxidation of mtDNA contributed to the upregulation of JMJD3 expression. Accordingly, the inflammation in the pancreas and lung was partially relieved after the treatment of NAC (Fig. 4G, Supplemental Figs. 2C, 4B), indicating the indispensable role of mtDNA oxidation in the induction of severe histopathological injury. The percentages of TNF-α^+ inflammatory monocytes were also decreased in the lung and peripheral blood of mice injected with NAC compared with that of the control (Fig. 4H, 4I). These results indicated that mitochondrial-derived DAMPs, including the oxidized form of mtDNA, play essential roles in the induction of severe pancreatic inflammation and lung injury. The inhibition of ROS by NAC in vivo decreased the oxidation of mtDNA in the circulating monocytes and resulted in the relief of pancreatic inflammation and lung injury.

AP and inflammation triggered by mtDNA and oxidized-mtDNA were alleviated in Sting$^{-/-}$ *and* Tlr9$^{-/-}$ *mice*

To further address the role of mtDNA, TLR9, and STING pathways in the occurrence of pulmonary injury in AP, we used *WT*, *Sting*$^{-/-}$, and *Tlr9*$^{-/-}$ mice to observe the inflammatory response in the lung in the Cae-induced disease model. As shown in Fig. 5A and

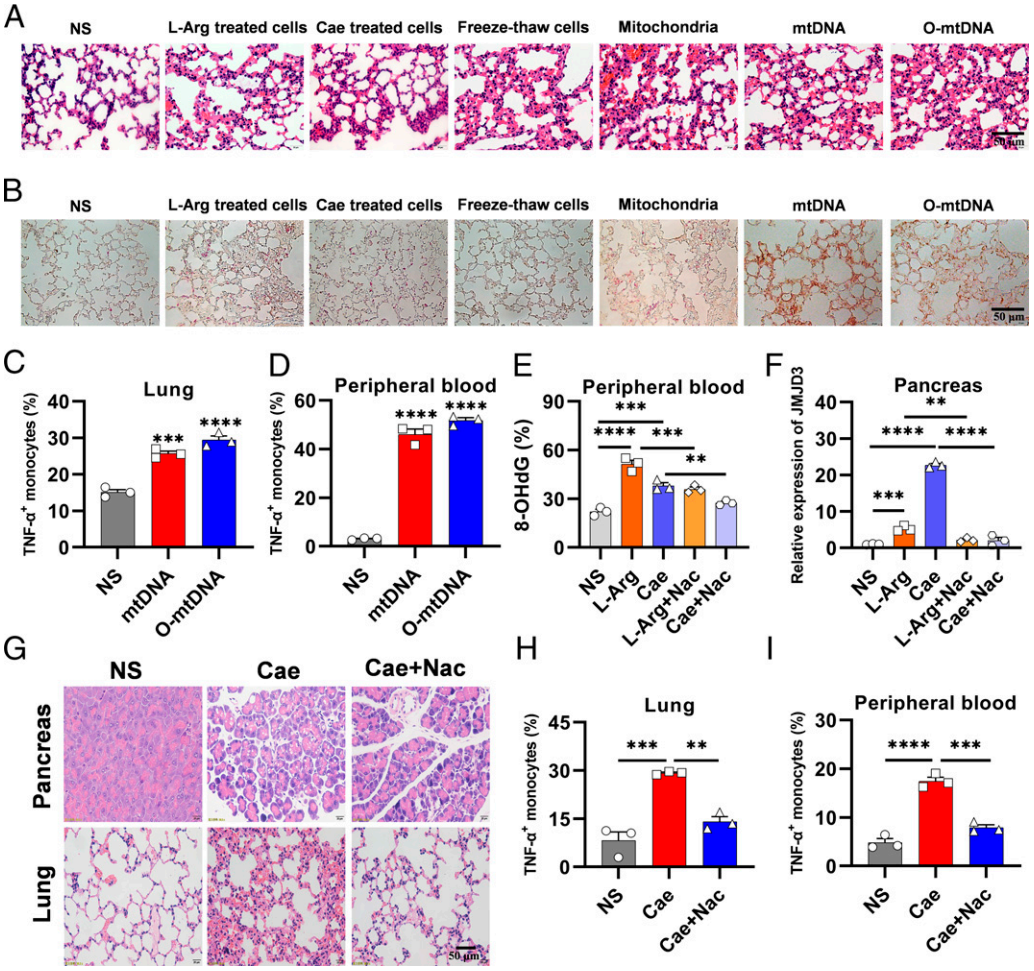

FIGURE 4. Mitochondrial content released by pancreatic acinar cells contributed to inflammation in mice with AP. (**A**) Representative H&E-stained sections of the lung from mice at 48 h after i.v. injection of pancreatic acinar cells treated with L-Arg or Cae, freeze-thaw cells, mitochondria, mtDNA, and oxidized-mtDNA (cells: 1×10^6/mouse, mitochondria: 200 μg/mouse, mtDNA and oxidized-mtDNA: 15 μg/mouse); original magnification ×400. (**B**) Specific esterase staining of neutrophils in mouse lung sections; original magnification ×400. (**C** and **D**) Percentages of TNF-α$^+$CD45$^+$CD11b$^+$Ly6C$^+$ inflammatory monocytes in mouse lung and peripheral blood at 24 h after the injection of NS, mtDNA (15 μg/mouse), or oxidized-mtDNA (15 μg/mouse). (**E**) Percentage of 8-OHdG$^+$ CD45$^+$CD11b$^+$Ly6C$^+$ inflammatory monocytes in peripheral blood of mice treated with NS, L-Arg, Cae, L-Arg+NAC, and Cae+NAC. (**F**) Relative expression of JMJD3 in the mouse pancreas. (**G**) Representative H&E-stained sections of the pancreas and lung from mice were injected i.p. with NAC after Cae administration. (**H** and **I**) The percentage of TNF-α$^+$CD45$^+$CD11b$^+$Ly6C$^+$ inflammatory monocytes in the lung and peripheral blood of mice. $^{**}p < 0.01$, $^{***}p < 0.001$, $^{****}p < 0.0001$.

Supplemental Figs. 2D and 4C, the pathological changes in the pancreas and lung were significantly reduced in *Sting*$^{-/-}$ and *Tlr9*$^{-/-}$ mice. The population of circulating inflammatory cells was decreased in both peripheral blood (Supplemental Fig. 1C) and infiltrated lung tissue (Fig. 5B). In addition, the percentages of TNF-α$^+$CD45$^+$ CD11b$^+$Ly6C$^+$ inflammatory monocytes in the lungs of *Sting*$^{-/-}$ and *Tlr9*$^{-/-}$ mice at 24 h after the administration of Cae were decreased compared with those in the lungs of *WT* mice (Fig. 5C). The critical role of mtDNA and oxidized-mtDNA in the induction of pulmonary inflammation was further studied by injection into *WT*, *Sting*$^{-/-}$, and *Tlr9*$^{-/-}$ mice. Forty-eight hours after the i.v. injection, *Sting*$^{-/-}$ and *Tlr9*$^{-/-}$ mice showed reduced pulmonary damage compared with *WT* mice (Fig. 5D, Supplemental Fig. 2E). The flow cytometry results revealed decreased percentages of monocytes and neutrophils in the lungs of *Tlr9*$^{-/-}$ and *Sting*$^{-/-}$ mice (Fig. 5E). Furthermore, the percentage of monocytes secreting TNF-α was decreased in the lungs of both *Tlr9*$^{-/-}$ and *Sting*$^{-/-}$ mice (Fig. 5F). These results further confirmed that mtDNA and oxidized-mtDNA promoted the inflammatory process of AP through the *Tlr9*$^{-/-}$ and *Sting*$^{-/-}$ pathways.

Inhibition of JMJD3 ameliorated AP in mice

To further study the role of JMJD3 in AP, we used the JMJD3-specific inhibitor GSK-J4 in mice with AP. As shown in Fig. 6A and Supplemental Figs. 3A and 4D, pathological lesions were alleviated in GSK-J4–treated groups compared with the AP control groups. In addition, the percentages of monocytes and neutrophils were detected in the pancreas, lung, and peripheral blood by flow cytometry. The results showed that the percentages of monocytes and neutrophils in the pancreas (Supplemental Fig. 1D), lung (Fig. 6B, top), and peripheral blood (Fig. 6B, bottom) of the GSK-J4–treated groups were lower than those of the AP control groups. The percentage of TNF-α$^+$CD45$^+$CD11b$^+$Ly6C$^+$ inflammatory monocytes in the pancreas (Supplemental Fig. 1E), lung (Fig. 6C, left), and peripheral blood (Fig. 6C, right) of mice injected with GSK-J4 at 24 h after the administration of AP were decreased compared with the control group. These data demonstrated that JMJD3 promoted the inflammatory process of AP, and inhibition of JMJD3 activity ameliorated AP and its related lung injury with a significant reduction in monocytes expressing TNF-α.

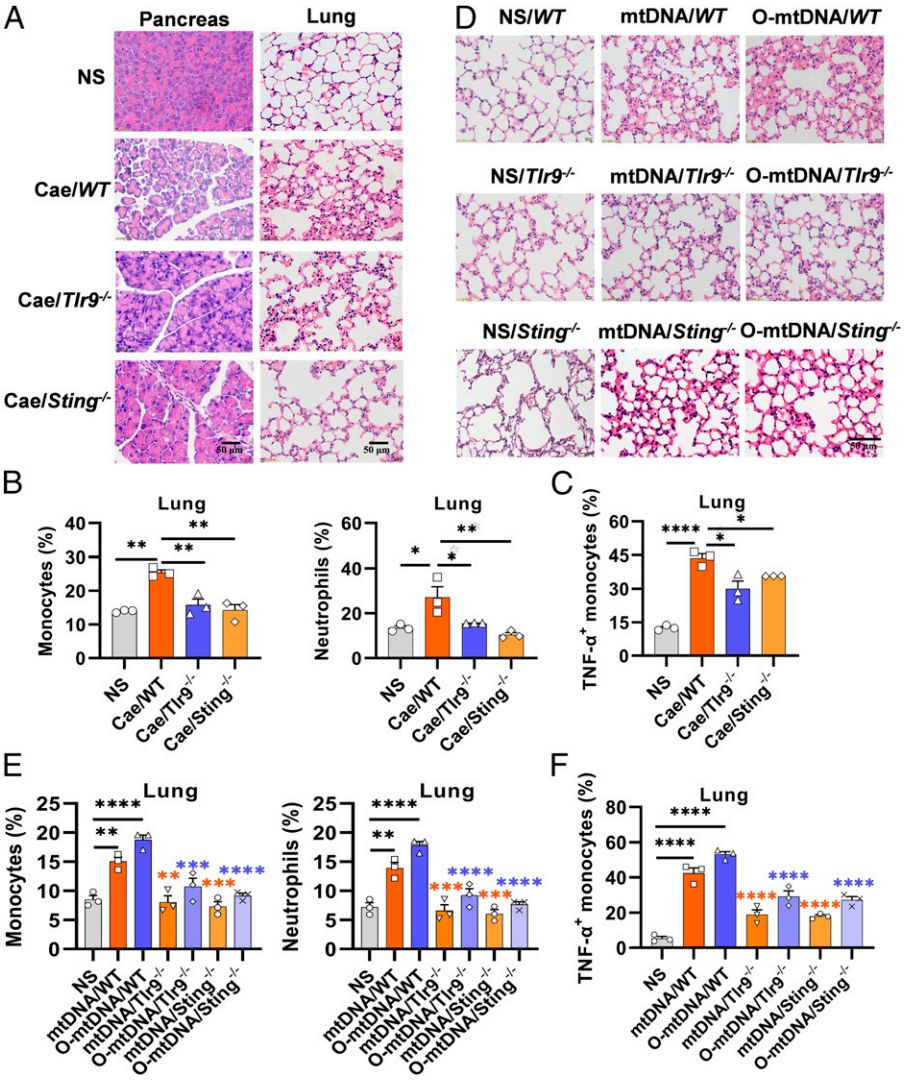

FIGURE 5. AP and inflammation triggered by mtDNA and oxidized-mtDNA were alleviated in *Sting*$^{-/-}$ *and Tlr9*$^{-/-}$ mice. (**A**) Representative H&E-stained sections of the lung and pancreas of *WT*, *Tlr9*$^{-/-}$, and *Sting*$^{-/-}$ mice at 48 h after Cae induced AP; original magnification ×400. (**B**) Percentages of infiltrating monocytes and neutrophils in the lungs of *WT*, *Tlr9*$^{-/-}$, and *Sting*$^{-/-}$ mice 48 h after Cae induced AP. (**C**) Percentages of TNF-α^{+}CD45^{+}CD11b^{+} Ly6C^{+} inflammatory monocytes in the lungs of *WT*, *Tlr9*$^{-/-}$, and *Sting*$^{-/-}$ mice at 24 h after Cae induced AP. (**D**) Representative H&E-stained sections of the lung from *WT*, *Tlr9*$^{-/-}$, and *Sting*$^{-/-}$ mice were i.v. injected with mtDNA and oxidized-mtDNA; original magnification ×400. (**E**) Percentages of infiltrating monocytes and neutrophils in the lungs of *WT*, *Tlr9*$^{-/-}$, and *Sting*$^{-/-}$ mice 48 h after the i.v. injection of mtDNA (15 μg/mouse) and oxidized-mtDNA (15 μg/mouse). (**F**) Percentages of TNF-α^{+} CD45^{+}CD11b^{+}Ly6C^{+} inflammatory monocytes in the lungs of *WT*, *Tlr9*$^{-/-}$, and *Sting*$^{-/-}$ mice at 24 h after the i.v. injection of mtDNA (15 μg/mouse) and oxidized-mtDNA (15 μg/mouse). The orange asterisks indicate the significant difference between mtDNA-treated *WT* mice and knockout mice; the slate blue asterisks indicate the significant difference between oxidized-mtDNA–treated *WT* mice and knockout mice. *$p < 0.05$, **$p < 0.01$, ***$p < 0.001$, ****$p < 0.0001$.

In the next experiment, AP was induced in *WT* and *Jmjd3-cKO* mice. As shown in Fig. 6D and Supplemental Figs. 3B and 4E, the pathological alterations of the pancreas and lung were significantly reduced in *Jmjd3-cKO* mice. The percentages of infiltrating monocytes and neutrophils in the pancreas (Supplemental Fig. 1F), lung (Fig. 6E, top), and peripheral blood (Fig. 6E, bottom) of *Jmjd3-cKO* mice were decreased compared with those of *WT* mice, and the percentage of TNF-α^{+} inflammatory monocytes was decreased (Fig. 6F). A similar tendency was observed in the experiment by administration of mtDNA and oxidized-mtDNA. Forty-eight hours after injection, the pulmonary inflammation of *Jmjd3-cKO* mice was alleviated compared with that of *WT* mice (Fig. 6G, Supplemental Fig. 3C). The flow cytometry results suggested decreased percentages of monocytes and neutrophils (Fig. 6H), as well as TNF-α^{+}CD45^{+}CD11b^{+}Ly6C^{+} inflammatory monocytes (Supplemental Fig. 1G), in the lungs of *Jmjd3-cKO* mice as compared with the control mice. These results demonstrated that JMJD3 plays an indispensable role in the induction of inflammation in AP and its lung injury.

Discussion

JMJD3 is a crucial histone demethylase for the regulation of several genes involved in inflammatory signaling pathways. JMJD3 is a potent enhancer of proinflammatory genes, mainly because of its participation in the NF-κB pathway (42). The reason why NF-κB directs the transcription of JMJD3 is that there are two conserved κB sites in the promoter sequences upstream of the first coding exon of JMJD3 (26). De Santa et al. (8) demonstrated that the effect of LPS on bone marrow–derived macrophages induced significant recruitment of NF-κB/p65 and JMJD3 to TNF-α transcription initiation sites. Das et al. (42) observed that the alteration of JMJD3 expression affected the transcription of a network of NF-κB–dependent genes in human leukemia monocyte macrophages. In view of the close relationship between NF-κB and JMJD3, we hypothesized that the NF-κB-JMJD3 pathway might play a critical role in AP.

Studies have shown that ROS is generated in the early stage of acute necrotizing pancreatitis, and the main target of ROS and redox signal transduction in AP is NF-κB. It has also been shown that nearly all pathways leading to NF-κB activation can be blocked by treatment with a variety of antioxidants, including NAC and glutathione (43, 44). However, the precise molecular mechanism of ROS that activates NF-κB needs further study in AP. mtDNA is particularly vulnerable to oxidative damage because it is close to ROS production sites and lacks histone protection (45). ROS generation is an important factor for the generation of 8-OHdG, and 8-OHdG can also be abundant under UV exposure (46). Increased levels of ROS produce oxidatively modified mtDNA in newly recruited inflammatory cells, and oxidized-mtDNA induces more production of inflammatory cytokines in immune cells through the TLR9/STING-NF-κB pathways (21, 23). In vitro and in vivo experiments showed that oxidized-mtDNA has

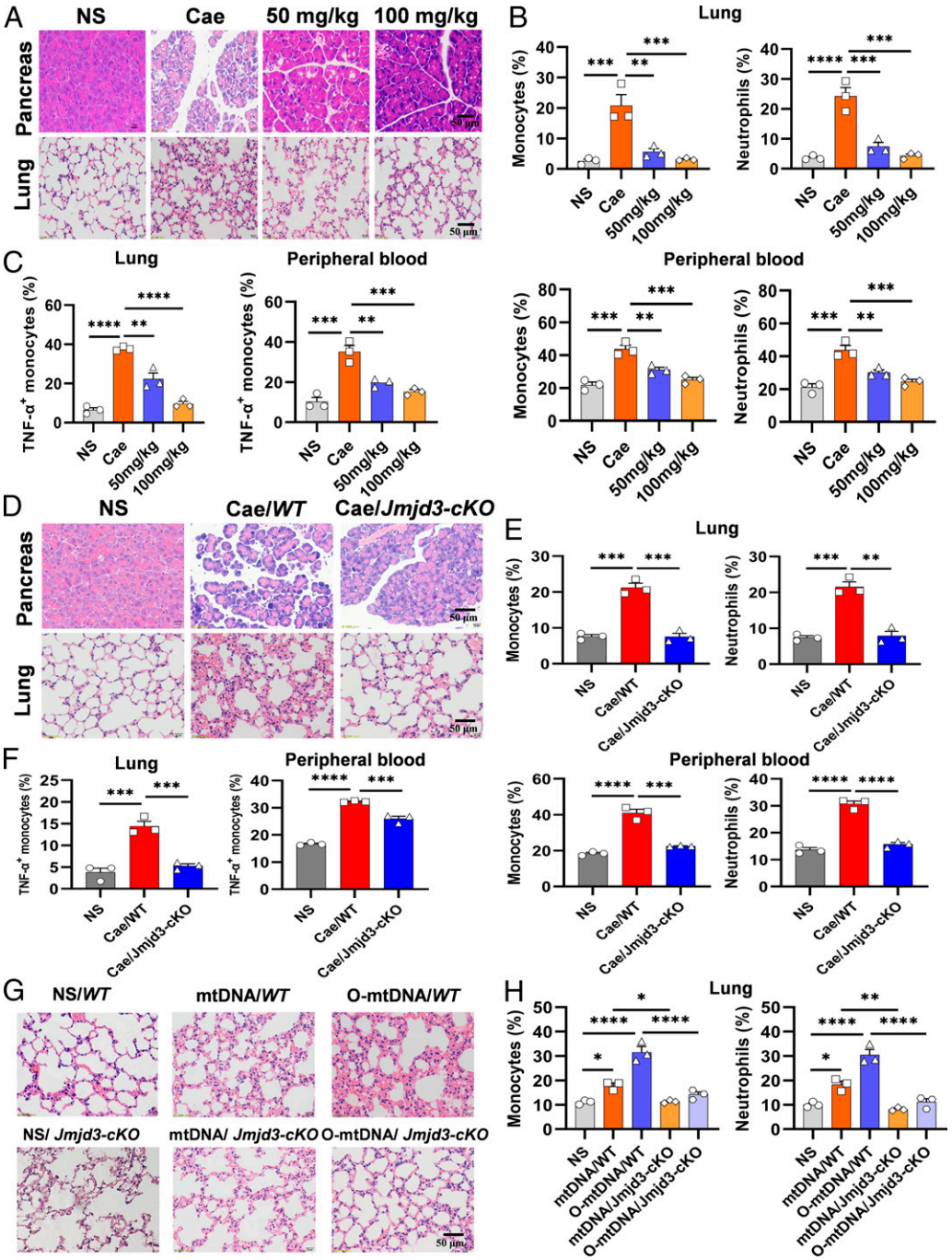

FIGURE 6. Inhibition of JMJD3 ameliorated AP in mice. Mice were divided into four groups: NS group, AP model group induced by Cae, AP model group i.p. injected with 50 mg/kg GSK-J4, and AP model group i.p. injected with 100 mg/kg GSK-J4. (**A**) Representative H&E-stained sections of the pancreas and lung at 48 h after the first injection of Cae; original magnification ×400. (**B**) Percentages of infiltrating monocytes and neutrophils in the lung and peripheral blood of mice at 48 h after the first injection of Cae. (**C**) Percentages of TNF-α^+CD45$^+$CD11b$^+$Ly6C$^+$ inflammatory monocytes in the lung and peripheral blood of mice at 24 h after the first injection of Cae. (**D**) Representative H&E-stained sections of the pancreas and lung of *WT* and *Jmjd3-cKO* mice at 48 h after the first injection of Cae; original magnification ×400. (**E**) Percentages of infiltrating monocytes and neutrophils in the lung and peripheral blood of *WT* and *Jmjd3-cKO* mice at 48 h after administration of Cae. (**F**) Percentages of TNF-α^+CD45$^+$CD11b$^+$Ly6C$^+$ infiltrating monocytes in the lung and peripheral blood at 24 h after the first injection of Cae. (**G**) Representative H&E-stained sections of the lung from *WT* and *Jmjd3-cKO* mice i.v. injected with mtDNA and oxidized-mtDNA; original magnification ×400. (**H**) Percentages of infiltrating monocytes and neutrophils in the lungs of *WT* and *Jmjd3-cKO* mice 48 h after the i.v. injection of mtDNA (15 μg/mouse) and oxidized-mtDNA (15 μg/mouse). $^*p < 0.05$, $^{**}p < 0.01$, $^{***}p < 0.001$, $^{****}p < 0.0001$.

greater potential to activate dendritic cells than natural mtDNA (21). According to the observations in previous studies, purified mtDNA or even oligodeoxynucleotide (ODN) contained a single 8-OHdG residue but lacked CpG motifs, inducing arthritis in mice after intra-articular injection. In contrast, ODNs lack the oxidized base but possess identical sequences that are completely inert in vivo, except for the lack of oxidative bases (47). In another study, a significantly higher amount of TNF-α was induced from RAW264.7 macrophage-like cells by the 8-OHdG–substituted CPG ODN molecule than that of nonsubstituted control cells. In primary cultured macrophages isolated from *WT* mice, an increase in TNF-α production induced by DNA containing 8-OHdG was also observed, but this increase was not

observed in *Tlr9*$^{-/-}$ mice. In addition, s.c. injection of 8-OHdG containing CpG ODN resulted in increased footpad swelling compared with regular CpG ODN (48).

In our research, JMJD3 was upregulated in the early stage of AP. This discovery prompted us to further explore the cause of elevated JMJD3 and its role in the inflammatory process of AP. mtDNA activates innate immunity by the TLR9/STING-NF-κB pathways (20), and mtDNA released from necrotic pancreatic cells has been reported as a marker of AP (49). This suggests that therapeutically targeting STING and TLR9 may be a promising approach for the treatment of severe AP (50, 51). Subsequently, we found that mtDNA stimulated the expression of JMJD3 in vitro and in vivo, and oxidized-mtDNA had a more stimulatory effect. Thus, we hypothesized that mtDNA and oxidized-mtDNA triggered the STING and TLR9 pathways and activated NF-κB p65. NF-κB p65 stimulated the expression of JMJD3, which promoted TNF-α secretion from monocytes in mice. To further confirm our hypothesis, we applied the JMJD3-specific inhibitor GSK-J4 and the ROS inhibitor NAC in AP mice. Both inhibitors ameliorated AP in mice and inhibited TNF-α secretion by monocytes. In addition, the amelioration of AP and inhibition of TNF-α secretion appeared in TLR9-, STING-, and JMJD3-deficient mice with AP. Interestingly, monocytes are the major subgroup of the predominant leukocyte subset, which upregulates JMJD3 during AP. Notably, our in vitro studies showed that mtDNA released by dead acinar cells activated JMJD3 in monocytes and stimulated the secretion of TNF-α. In AP models, except for the STING and TLR9 pathways reported in this study mediating TNF-α secretion, the other TLRs, including TLR2 and TLR4, are essential for the activation of proinflammatory pathways. Stimulation of TLR4 plays a significant proinflammatory role, which subsequently induces the production of inflammatory cytokines such as IL-1β and IL-6 (52). Nevertheless, a general consensus has not been achieved because controversial outcomes were presented, and in-depth elucidation of the mechanism is warranted (53).

As with the majority of studies, the design of this study is subject to limitations. There are two major limitations in this study that could be addressed in future research. First, the study focused only on C57BL/6 male mice. It is reported that Cae is a cholecystokinin-pancreozymin analog and is used to successfully cause AP in male mice, which belongs to a hormone-induced model (54). In addition, the effects of estrogens in female mice in the setting of AP are complex and vary with sex (55). To avoid the influence of estrogens in female mice, male mice are favorably used to establish the AP model compared with the female ones (56). Although animal studies on pancreatitis typically use male animals, animal studies using both males and females, or with sex hormone treatment, also suggest that sex may play a role in the development of AP (56). Whether sex differences exist for the endogenous inhibitors of the pancreas is unknown, providing valuable insight to conduct relevant in-depth research. Second, the study focused on the crucial role of JMJD3 and related pathways in AP and pancreatitis-associated lung injury, aiming to provide therapeutic strategies for the treatment of pancreatitis. Whether the effect of JMJD3 on pancreatitis is specific is a point worthy of attention in subsequent studies.

In summary, these findings indicate that JMJD3 is crucial in the development of AP via the TLR9 and STING pathways, which are activated by mtDNA and oxidized-mtDNA released from acinar cell death. Our study suggested that targeted therapies targeting JMJD3 in monocytes might prove beneficial in AP treatment and might provide insight into the development of novel therapeutic agents for other inflammatory diseases.

Study approval

All animal experiments were performed according to the guidelines of the Institutional Animal Care and Use Committee of Sichuan University (Chengdu, Sichuan, China), and the protocols were approved by the Institutional Animal Care and Use Committee of Sichuan University. Surgical incision tissue from CP patients was provided by West China Hospital of Sichuan University. Written informed consent was received from participants before inclusion in the study. This study was performed in strict accordance with recommendations from the Medical Ethics Committee of the West China Hospital of Sichuan University (2014, No. 37).

Disclosures

The authors have no financial conflicts of interest.

References

1. da Costa, D. W., D. Boerma, H. C. van Santvoort, K. D. Horvath, J. Werner, C. R. Carter, T. L. Bollen, H. G. Gooszen, M. G. Besselink, and O. J. Bakker. 2014. Staged multidisciplinary step-up management for necrotizing pancreatitis. *Br. J. Surg.* 101: e65–e79.
2. Sabo, A., N. Goussous, N. Sardana, S. Patel, and S. C. Cunningham. 2015. Necrotizing pancreatitis: a review of multidisciplinary management. *JOP* 16: 125–135.
3. Moggia, E., R. Koti, A. P. Belgaumkar, F. Fazio, S. P. Pereira, B. R. Davidson, and K. S. Gurusamy. 2017. Pharmacological interventions for acute pancreatitis. *Cochrane Database Syst. Rev.* 4: CD011384.
4. Wang, G., Y. Liu, S. F. Zhou, P. Qiu, L. Xu, P. Wen, J. Wen, and X. Xiao. 2016. Effect of somatostatin, ulinastatin and gabexate on the treatment of severe acute pancreatitis. *Am. J. Med. Sci.* 351: 506–512.
5. Dawra, R., R. Sharif, P. Phillips, V. Dudeja, D. Dhaulakhandi, and A. K. Saluja. 2007. Development of a new mouse model of acute pancreatitis induced by administration of L-arginine. *Am. J. Physiol. Gastrointest. Liver Physiol.* 292: G1009–G1018.
6. Agger, K., P. A. Cloos, J. Christensen, D. Pasini, S. Rose, J. Rappsilber, I. Issaeva, E. Canaani, A. E. Salcini, and K. Helin. 2007. UTX and JMJD3 are histone H3K27 demethylases involved in HOX gene regulation and development. *Nature* 449: 731–734.
7. Salminen, A., K. Kaarniranta, M. Hiltunen, and A. Kauppinen. 2014. Histone demethylase Jumonji D3 (JMJD3/KDM6B) at the nexus of epigenetic regulation of inflammation and the aging process. *J. Mol. Med. (Berl.)* 92: 1035–1043.
8. De Santa, F., M. G. Totaro, E. Prosperini, S. Notarbartolo, G. Testa, and G. Natoli. 2007. The histone H3 lysine-27 demethylase Jmjd3 links inflammation to inhibition of polycomb-mediated gene silencing. *Cell* 130: 1083–1094.
9. Kruidenier, L., C. W. Chung, Z. Cheng, J. Liddle, K. Che, G. Joberty, M. Bantscheff, C. Bountra, A. Bridges, H. Diallo, et al. 2012. A selective jumonji H3K27 demethylase inhibitor modulates the proinflammatory macrophage response. *Nature* 488: 404–408.
10. Lee, P. J., and G. I. Papachristou. 2019. New insights into acute pancreatitis. *Nat. Rev. Gastroenterol. Hepatol.* 16: 479–496.
11. Sendler, M., A. Dummer, F. U. Weiss, B. Krüger, T. Wartmann, K. Scharffetter-Kochanek, N. van Rooijen, S. R. Malla, A. Aghdassi, W. Halangk, et al. 2013. Tumour necrosis factor α secretion induces protease activation and acinar cell necrosis in acute experimental pancreatitis in mice. *Gut* 62: 430–439.
12. Han, J. M., E. K. Lee, S. Y. Gong, J. K. Sohng, Y. J. Kang, and H. J. Jung. 2019. Sparassis crispa exerts anti-inflammatory activity via suppression of TLR-mediated NF-κB and MAPK signaling pathways in LPS-induced RAW264.7 macrophage cells. *J. Ethnopharmacol.* 231: 10–18.
13. Wang, Y. Y., D. Shen, L. J. Zhao, N. Zeng, and T. H. Hu. 2019. Sting is a critical regulator of spinal cord injury by regulating microglial inflammation via interacting with TBK1 in mice. *Biochem. Biophys. Res. Commun.* 517: 741–748.
14. Chan, L. K., M. Gerstenlauer, B. Konukiewitz, K. Steiger, W. Weichert, T. Wirth, and H. J. Maier. 2017. Epithelial NEMO/IKKγ limits fibrosis and promotes regeneration during pancreatitis. *Gut* 66: 1995–2007.
15. Chen, X., M. Xiu, J. Xing, S. Yu, D. Min, and F. Guo. 2017. Lanthanum chloride inhibits LPS mediated expressions of pro-inflammatory cytokines and adhesion molecules in HUVECs: involvement of NF-κB-Jmjd3 signaling. *Cell. Physiol. Biochem.* 42: 1713–1724.
16. Wei, Y., R. Chen, S. Dimicoli, C. Bueso-Ramos, D. Neuberg, S. Pierce, H. Wang, H. Yang, Y. Jia, H. Zheng, et al. 2013. Global H3K4me3 genome mapping reveals alterations of innate immunity signaling and overexpression of JMJD3 in human myelodysplastic syndrome CD34+ cells. *Leukemia* 27: 2177–2186.
17. Taminiau, A., A. Draime, J. Tys, B. Lambert, J. Vandeputte, N. Nguyen, P. Renard, D. Geerts, and R. Rezsöhazy. 2016. HOXA1 binds RBCK1/HOIL-1 and TRAF2 and modulates the TNF/NF-κB pathway in a transcription-independent manner. *Nucleic Acids Res.* 44: 7331–7349.
18. Habtezion, A., A. S. Gukovskaya, and S. J. Pandol. 2019. Acute pancreatitis: a multifaceted set of organelle and cellular interactions. *Gastroenterology* 156: 1941–1950.
19. Wei, X., B. Shao, Z. He, T. Ye, M. Luo, Y. Sang, X. Liang, W. Wang, S. Luo, S. Yang, et al. 2015. Cationic nanocarriers induce cell necrosis through impairment of Na(+)/K(+)-ATPase and cause subsequent inflammatory response. *Cell Res.* 25: 237–253.

20. Fang, C., X. Wei, and Y. Wei. 2016. Mitochondrial DNA in the regulation of innate immune responses. *Protein Cell* 7: 11–16.
21. Pazmandi, K., Z. Agod, B. V. Kumar, A. Szabo, T. Fekete, V. Sogor, A. Veres, I. Boldogh, E. Rajnavolgyi, A. Lanyi, and A. Bacsi. 2014. Oxidative modification enhances the immunostimulatory effects of extracellular mitochondrial DNA on plasmacytoid dendritic cells. *Free Radic. Biol. Med.* 77: 281–290.
22. Caielli, S., S. Athale, B. Domic, E. Murat, M. Chandra, R. Banchereau, J. Baisch, K. Phelps, S. Clayton, M. Gong, et al. 2016. Oxidized mitochondrial nucleoids released by neutrophils drive type I interferon production in human lupus. *J. Exp. Med.* 213: 697–713.
23. Lood, C., L. P. Blanco, M. M. Purmalek, C. Carmona-Rivera, S. S. De Ravin, C. K. Smith, H. L. Malech, J. A. Ledbetter, K. B. Elkon, and M. J. Kaplan. 2016. Neutrophil extracellular traps enriched in oxidized mitochondrial DNA are interferogenic and contribute to lupus-like disease. *Nat. Med.* 22: 146–153.
24. Banks, P. A., T. L. Bollen, C. Dervenis, H. G. Gooszen, C. D. Johnson, M. G. Sarr, G. G. Tsiotos, S. S. Vege; Acute Pancreatitis Classification Working Group. 2013. Classification of acute pancreatitis—2012: revision of the Atlanta classification and definitions by international consensus. *Gut* 62: 102–111.
25. Du, D., L. Yao, R. Zhang, N. Shi, Y. Shen, X. Yang, X. Zhang, T. Jin, T. Liu, L. Hu, et al. 2018. Protective effects of flavonoids from Coreopsis tinctoria Nutt. on experimental acute pancreatitis via Nrf-2/ARE-mediated antioxidant pathways. *J. Ethnopharmacol.* 224: 261–272.
26. Perides, G., E. R. Weiss, E. S. Michael, J. M. Laukkarinen, J. S. Duffield, and M. L. Steer. 2011. TNF-alpha-dependent regulation of acute pancreatitis severity by Ly-6C(hi) monocytes in mice. *J. Biol. Chem.* 286: 13327–13335.
27. Kasper, M., K. Walscheid, B. Laffer, D. Bauer, M. Busch, L. Wildschütz, B. Wang, K. Loser, T. Vogl, R. S. Grajewski, et al. 2018. The phenotype of monocytes in anterior uveitis depends on the HLA-B27 status. *Front. Immunol.* 9: 1773.
28. Lee, S., K. Nakahira, J. Dalli, I. I. Siempos, P. C. Norris, R. A. Colas, J. S. Moon, M. Shinohara, S. Hisata, J. A. Howrylak, et al. 2017. NLRP3 inflammasome deficiency protects against microbial sepsis via increased lipoxin B_4 synthesis. *Am. J. Respir. Crit. Care Med.* 196: 713–726.
29. 2018. Blood monocyte frequency may be a biomarker for response to anti-PD-1. *Cancer Discov.* 8: 265.
30. Liu, L., Y. Liu, B. Xu, C. Liu, Y. Jia, T. Liu, C. Fang, W. Wang, J. Ren, Z. He, et al. 2018. Negative regulation of cationic nanoparticle-induced inflammatory toxicity through the increased production of prostaglandin E2 via mitochondrial DNA-activated $Ly6C^+$ monocytes. *Theranostics* 8: 3138–3152.
31. Chen, Y., S. Zhang, G. Peng, J. Yu, T. Liu, R. Meng, Z. Li, Y. Zhao, and G. Wu. 2013. Endothelial NO synthase and reactive oxygen species mediated effect of simvastatin on vessel structure and function: pleiotropic and dose-dependent effect on tumor vascular stabilization. *Int. J. Oncol.* 42: 1325–1336.
32. Wilhelm, J., R. Vytášek, J. Uhlík, and L. Vajner. 2016. Oxidative stress in the developing rat brain due to production of reactive oxygen and nitrogen species. *Oxid. Med. Cell. Longev.* 2016: 5057610.
33. Schmidt, J., D. W. Rattner, K. Lewandrowski, C. C. Compton, U. Mandavilli, W. T. Knoefel, and A. L. Warshaw. 1992. A better model of acute pancreatitis for evaluating therapy. *Ann. Surg.* 215: 44–56.
34. Liu, L., Q. Wei, Q. Lin, J. Fang, H. Wang, H. Kwok, H. Tang, K. Nishiura, J. Peng, Z. Tan, et al. 2019. Anti-spike IgG causes severe acute lung injury by skewing macrophage responses during acute SARS-CoV infection. *JCI Insight* 4: e123158.
35. Tamizhselvi, R., P. K. Moore, and M. Bhatia. 2007. Hydrogen sulfide acts as a mediator of inflammation in acute pancreatitis: in vitro studies using isolated mouse pancreatic acinar cells. *J. Cell. Mol. Med.* 11: 315–326.
36. Huang, N., G. Murtaza, L. Wang, J. Luan, X. Wang, Y. Sun, X. Wu, Y. Tao, S. Shi, P. Cao, et al. 2020. Chrm3 protects against acinar cell necrosis by stabilizing caspase-8 expression in severe acute pancreatitis mice model. *J. Cell. Biochem.* 121: 2618–2631.
37. Jia, R., J. Ma, W. Meng, and N. Wang. 2018. Dihydromyricetin inhibits caerulin-induced TRAF3-p38 signaling activation and acute pancreatitis response. *Biochem. Biophys. Res. Commun.* 503: 1696–1702.
38. Li, C., and H. Wang. 2015. Selective enzymatic cleavage and labeling for sensitive capillary electrophoresis laser-induced fluorescence analysis of oxidized DNA bases. *J. Chromatogr. A* 1406: 324–330.
39. Ehlers, R. A., A. Hernandez, L. S. Bloemendal, R. T. Ethridge, B. Farrow, and B. M. Evers. 1999. Mitochondrial DNA damage and altered membrane potential (delta psi) in pancreatic acinar cells induced by reactive oxygen species. *Surgery* 126: 148–155.
40. Hauser, C. J., and L. E. Otterbein. 2018. Danger signals from mitochondrial DAMPS in trauma and post-injury sepsis. *Eur. J. Trauma Emerg. Surg.* 44: 317–324.
41. Jin, H. Z., X. J. Yang, K. L. Zhao, F. C. Mei, Y. Zhou, Y. D. You, and W. X. Wang. 2019. Apocynin alleviates lung injury by suppressing NLRP3 inflammasome activation and NF-κB signaling in acute pancreatitis. *Int. Immunopharmacol.* 75: 105821.
42. Das, N. D., K. H. Jung, M. R. Choi, H. S. Yoon, S. H. Kim, and Y. G. Chai. 2012. Gene networking and inflammatory pathway analysis in a JMJD3 knockdown human monocytic cell line. *Cell Biochem. Funct.* 30: 224–232.
43. Fu, J., Q. Shi, X. Song, X. Xia, C. Su, Z. Liu, E. Song, and Y. Song. 2016. Tetrachlorobenzoquinone exhibits neurotoxicity by inducing inflammatory responses through ROS-mediated IKK/IκB/NF-κB signaling. *Environ. Toxicol. Pharmacol.* 41: 241–250.
44. Ma, Z., G. Song, D. Zhao, D. Liu, X. Liu, Y. Dai, Z. He, D. Qian, J. Gong, H. Meng, et al. 2019. Bone marrow-derived mesenchymal stromal cells ameliorate severe acute pancreatitis in rats via hemeoxygenase-1-mediated anti-oxidant and anti-inflammatory effects. *Cytotherapy* 21: 162–174.
45. Huang, H., and K. G. Manton. 2004. The role of oxidative damage in mitochondria during aging: a review. *Front. Biosci.* 9: 1100–1117.
46. Gehrke, N., C. Mertens, T. Zillinger, J. Wenzel, T. Bald, S. Zahn, T. Tüting, G. Hartmann, and W. Barchet. 2013. Oxidative damage of DNA confers resistance to cytosolic nuclease TREX1 degradation and potentiates STING-dependent immune sensing. *Immunity* 39: 482–495.
47. Collins, L. V., S. Hajizadeh, E. Holme, I. M. Jonsson, and A. Tarkowski. 2004. Endogenously oxidized mitochondrial DNA induces in vivo and in vitro inflammatory responses. *J. Leukoc. Biol.* 75: 995–1000.
48. Yoshida, H., M. Nishikawa, T. Kiyota, H. Toyota, and Y. Takakura. 2011. Increase in CpG DNA-induced inflammatory responses by DNA oxidation in macrophages and mice. *Free Radic. Biol. Med.* 51: 424–431.
49. Wu, L., W. Xu, F. Wang, T. Lv, Z. Yin, and Y. Song. 2018. Plasma mtDNA analysis aids in predicting pancreatic necrosis in acute pancreatitis patients: a pilot study. *Dig. Dis. Sci.* 63: 2975–2982.
50. Yan, Y., B. Lu, P. Li, and J. Wang. 2017. NOD receptor and TLR9 modulation in severe acute pancreatitis-induced intestinal injury. *Mol. Med. Rep.* 16: 8471–8476.
51. Zhao, Q., Y. Wei, S. J. Pandol, L. Li, and A. Habtezion. 2018. STING signaling promotes inflammation in experimental acute pancreatitis. *Gastroenterology* 154: 1822–1835.e2.
52. Wang, Y., Y. Cui, F. Cao, Y. Qin, W. Li, and J. Zhang. 2015. Ganglioside GD1a suppresses LPS-induced pro-inflammatory cytokines in RAW264.7 macrophages by reducing MAPKs and NF-κB signaling pathways through TLR4. *Int. Immunopharmacol.* 28: 136–145.
53. Vaz, J., H. Akbarshahi, and R. Andersson. 2013. Controversial role of toll-like receptors in acute pancreatitis. *World J. Gastroenterol.* 19: 616–630.
54. Su, K. H., C. Cuthbertson, and C. Christophi. 2006. Review of experimental animal models of acute pancreatitis. *HPB (Oxford)* 8: 264–286.
55. Wang, M., F. Gorelick, and A. Bhargava. 2021. Sex differences in the exocrine pancreas and associated diseases. *Cell. Mol. Gastroenterol. Hepatol.* 12: 427–441.
56. Drake, M., S. J. Dodwad, J. Davis, L. S. Kao, Y. Cao, and T. C. Ko. 2021. Sex-related differences of acute and chronic pancreatitis in adults. *J. Clin. Med.* 10: 300.